Interleaved boost converter voltage regulation using hybrid ANFIS-PID controller for off-grid microgrid

Linus Alwal Aloo, Peter Kamita Kihato, Stanley Irungu Kamau, Roy Sam Orenge
Department of Electrical and Electronic Engineering, Jomo Kenyatta University of Agriculture & Technology (JKUAT), Nairobi, Kenya

Article Info	ABSTRACT
	The utilization of a microgrid with a photovoltaic (PV) and wind generation system presents a challenge due to their voltage and power output variations. This problem is majorly addressed within the converter section of the microgrid using maximum power point tracking (MPPT) algorithms and voltage regulation strategies. This paper presents an interleaved boost converter (IBC) modeling and voltage control using a hybrid adaptive neuro-fuzzy inference system-proportional plus integral plus derivative (ANFIS-PID) controller for an off-grid microgrid. The modeling used the interleaving technique to obtain the microgrid's transfer function (TF) and case study simulation models within MATLAB and Simulink environments. The performance of the ANFIS-PID controller, which regulates voltage in the microgrid, was compared to that of the traditional proportional integral (PI) controller. Results indicated that the hybrid ANFIS-PID controller performed better than the PI controller in terms of reduced settling time, overshoot, rise time, and the ability to address the nonlinear dynamics of the microgrid.

Corresponding Author:

Linus Alwal Aloo
Department of Electrical and Electronic Engineering
Jomo Kenyatta University of Agriculture & Technology (JKUAT)
Nairobi, Kenya
Email: laloo@jkuat.ac.ke

1. INTRODUCTION

The main challenge regarding photovoltaic (PV) and wind generation system as sources of clean energy is their intermittency leading to a variable output, which cannot be easily predicted [1]–[3]. A microgrid is a type of autonomous grid containing various distributed generation (DG) micro sources, power conditioning technology, loads, and storage energy devices [4]–[6]. There are different views of a microgrid in terms of capacity. In this study, a microgrid is considered a small controllable power system whose nominal power output is $10\ kW$. Several studies have been conducted on modeling PV-wind microgrid energy system components [7]–[9]. Research by Meng *et al.* [10] presents the lithium-ion battery modeling with state of charge (SoC) estimation. The concepts concerning the DC-DC boost converter modeling are introduced by Rahim and Wang [11], where a step-up DC-DC boost converter with model predictive control (MPC) maximum power point tracking (MPPT) algorithm is applied to a PV system. However, the variable switching frequencies created problems of optimum design, and no interleaving was used. Research by Faraj and Hussein [12] compares the performance of interleaved DC-DC boost converter to that of the traditional boost DC-DC converter. In contrast, interleaved boost converter (IBC) is compared with Cuk Converter for PV systems by Tayade and Mopari [13] both of which reinforced the benefits of IBC. Research by Prabhakaran and Agarwal [14] applied a boost-single ended primary inductance converter (SEPIC) type Interleaved DC-DC converter to a bipolar DC microgrid. At

the same time, the three-phase parallel IBC designed by Hisar [15] demonstrates how output ripples are reduced when the number of parallel converters is increased.

Different types of MPPT algorithms are presented for PV systems by Özel and Karaaslan [16] and Alzubaidi *et al.* [17] and for the wind energy conversion system (WECS) by Tounsi *et al.* [18]. Research by Fouad *et al.* [19] presented modeling of microgrid system components using MATLAB/Simulink. However, it has not presented the mathematical equations or equivalent circuit models, nor has the interleaving technique been applied. The system advisor model [20] presented a platform to access technical details of actual microgrid components, while Kumar [21] introduced battery charging and discharging dynamics. Research by Sumarmad *et al.* [22] proposed proportional plus integral plus derivative (PID), fuzzy logic control (FLC), and artificial neural network (ANN) algorithms for voltage regulation in a hybrid microgrid system. The MPPT controller is based on the P&O method. The results obtained using MATLAB/Simulink indicated that the FLC outperformed the PID and ANN by registering a higher precision and efficiency. Research by Gamage *et al.* [23] designed an adaptive neuro-fuzzy inference system (ANFIS) controller for an off-grid PV microgrid with a battery and supercapacitor. The simulated results depicted better performance of the ANFIS in voltage regulation. Truong *et al.* [24] controlled the inverter DC voltage in a solar and wind grid-tie system using an ANFIS controller. The ANFIS controller performed better than the proportional integral (PI) controller in reducing overshoot and settling time. Research by Pawar and Nema [25], report the successful utilization of the ANFIS controller in energy prediction for a PV system.

From the reviewed literature, it is clear that a microgrid control system's success relies on the accuracy and dependency of the microgrid model and controller. Conventional control methods for regulating microgrid voltage and frequency, such as PI control, require accurate mathematical models of the microgrid. On the other hand, artificial intelligence-based control strategies such as ANN and FLC based methods do not require accurate mathematical models of the microgrid. They can handle the nonlinear dynamics of the system. In terms of interleaving technique, some existing models have not used the DC-DC converter interleaving technique, such as [4], [5], while in [7], only inverters are interleaved. From the perspective of control (MPPT) algorithms, some existing models only have MPPT on the PV side, such as [9], while some have neither used the interleaving technique nor the ANFIS-PID. This study considered the modeling and designing an IBC for a hybrid PV-wind microgrid using the interleaving technique and the ANFIS-PID controller. Apart from using the interleaving technique for micro sources, converters, and storage, the proposed model has an ANFIS-PID controller for both PV and wind side DC-DC converters. The DC-DC boost converter was modified by incorporating an RC circuit parallel to the output capacitor.

The major contributions of this work include the following: i) the interleaved DC-DC boost converter (IBC) model for PV-wind microgrid has been developed and ii) the proposed ANFIS-PID controller to optimize the IBC outputs in the microgrid. The remaining sections of this paper are arranged as follows: section 2 captures the method, which includes the microgrid system, IBC, battery energy storage system (BESS), ANFIS-PID, and the case study microgrid model. Section 3 covers results and discussions, and finally, section 4 gives the conclusions.

2. METHOD
2.1. Hybrid photovoltaic-wind microgrid system
The schematic model of the studied PV-wind hybrid microgrid and the individual components' transfer function (TF) based on small-signal low-order dynamic models is shown in Figure 1. It has a solar PV array system that mainly uses solar irradiance to generate DC power channeled to the DC-DC converter. The measured voltage and current are fed to the ANFIS-PID controller to control the DC-DC converter. At the same time, a permanent magnet synchronous generator (PMSG) based wind turbine (WT) uses wind speed to produce AC power. The PMSG's output is rectified and measured for channeling to the ANFIS-PID controller while simultaneously injecting it into the DC-DC converter.

2.2. Photovoltaic and wind turbine generation system modeling
The PV system is modeled starting from the cell (rated at about 0.5 V). The PV cell output current I_{PV} is coupled to the output voltage V_{PV}, by a nonlinear mathematical exponential expression in (1) [6], [11]:

$$I_{PV} = I_{Ph} - I_{D1} - I_{D2} - I_{sh} = I_{Ph} - I_{D1} - I_{D2} - \frac{(V_{PV} + I_{PV} R_s)}{R_{sh}} \qquad (1)$$

Where PV current due to irradiation, I_{Ph} is given by (2):

$$I_{Ph} = [I_{Ph-STC} + K_s(T_C - T_{STC})] \times (\frac{G}{G_{STC}}) \qquad (2)$$

Where I_{D1} and I_{D2} are respectively the currents through the first and second diodes, R_s is series resistance, R_{sh} is parallel resistance, T_{STC} is temperature at standard test condition (STC is $298 \ K$), I_{Ph-STC} is PV current at STC, T_C is ambient temperature, K_s is coefficient of short-circuit current, G is solar radiation, G_{STC} is solar irradiance at STC is $(1,000 \ W/m^2)$.

The PV system has been modeled using an equivalent circuit at the cell level based on the two-diode model to achieve better accuracy and increased power extraction [11]. The PV array system's maximum power point (MPP) voltage is fed to the IBC with the ANFIS-PID algorithm. The case study model of a $10 \ kW$ PV system microgrid was created in MATLAB/Simulink from a type A panel (Jinko solar JKM310M-72 panel), each with 72 cells, a peak voltage of $37.4 \ V$, a peak current of $8.29 \ A$ and power output of $310 \ W$ [20]. The aerodynamic WT power, P_m, of the WT, is specified by the cubic relationship (3):

$$P_m = \frac{1}{2}\rho A v^3 C_p(\lambda, \beta) \tag{3}$$

Where ρ is the air density of the generation site (kg/m^3), the area covered by the rotor blades, A is πR^2; R is the WT rotor radius in meters (m), v is the site wind speed (m/s), C_p, is the conversion efficiency or power coefficient of the wind power defined by the blade pitch angle β and the tip speed ratio of rotor blades λ [8]. According to Betz, C_p, is limited to 0.59 [18]. The power coefficient $C_p(\lambda, \beta)$ can be computed from (4) [18]:

$$C_p(\lambda, \beta) = C_1 \left(C_2 \frac{1}{\lambda_i} - C_3\beta - C_4 \right) exp \left(\frac{-C_5}{\lambda_i} \right) + C_6 \lambda \tag{4}$$

Where C_1, C_2, C_3, C_4, C_5 and C_6 are coefficients to be specified for a given WT, and the parameter λ_i is defined as (5) [4], [8], [18]:

$$\frac{1}{\lambda_i} = \frac{1}{(\lambda + 0.08\beta)} - \frac{0.035}{\beta^3 + 1} \tag{5}$$

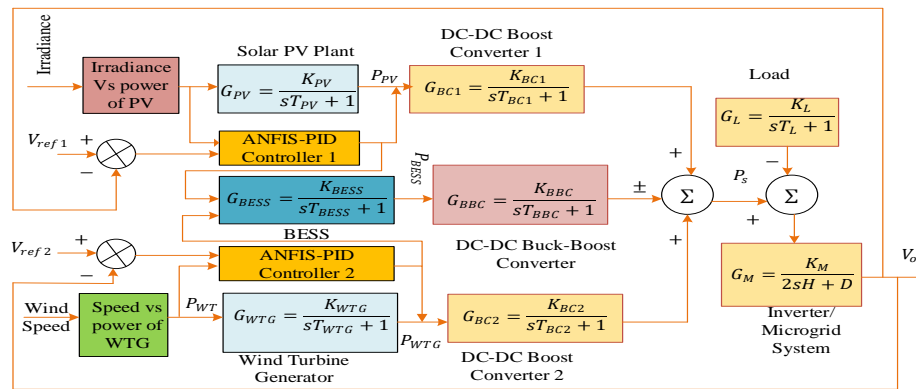The case study was created around a type A PMSG WT (westwind $6.4 \ m, 10 \ kW$) rated at $11.48 \ kW$.

Figure 1. Schematic model of the proposed PV-wind hybrid microgrid

2.3. Modeling of battery energy storage system

The BESS is a crucial component in a PV-wind hybrid microgrid. The BESS model is based on the lithium-ion battery and uses (6) and (7) [10], [21]:
Discharge model $(i^* > 0)$:

$$f_1(it, i^*, i,) = E_0 - K.\frac{Q}{Q - it}.i^* - K.\frac{Q}{Q - it}.it + A.exp(-B.it) \tag{6}$$

Charge model $(i^* < 0)$ [11], [26]:

$$f_2(it, i^*, i,) = E_0 - K.\frac{Q}{|it| + 0.1.Q}.i^* - K.\frac{Q}{Q - it}.it + A.exp(-B.it) \tag{7}$$

Where A is exponential voltage, in V, Q is battery capacity (Ahr), B is exponential capacity, in Ah^{-1}, E_0 is battery full capacity open-circuit voltage (OCV), K is coefficient of polarization resistance (Ω), I is battery

current (A), it is $\int i.dt$ (Ahr), and E_{bat} is nonlinear voltage (V). MATLAB/Simulink was used to create the BESS model using (6) and (7) and information gathered from a few pieces of literature, particularly from [21]. All the charge/discharge parameters were verified against the existing manufacturer's data sheets and literature [10], [20], [21].

2.4. Mathematical modeling and design of interleaved dc-dc boost converter

A microgrid that contains a PV system and wind energy produces the least voltage output, and as such, the boost converter circuit is required to give a sufficient voltage at the output side [11]. The advantages of boost converters include high efficiency, ease of control, and integration [12]. The IBC has been adopted in this study. A more accurate boost converter circuit was modified by incorporating an RC circuit in parallel with the output capacitor, as shown in Figure 2.
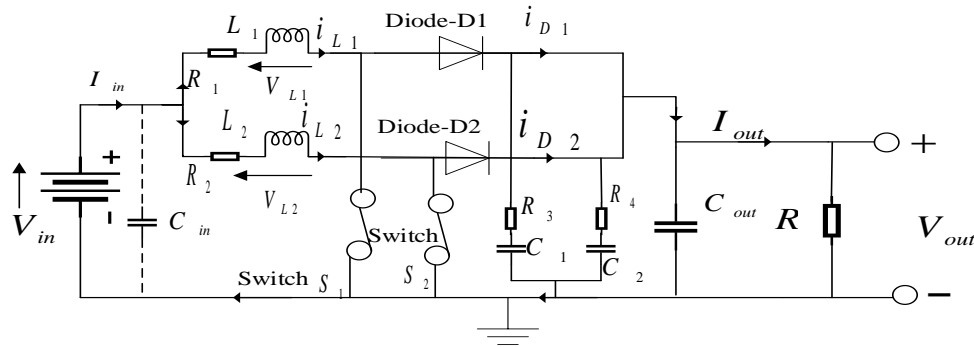

Figure 2. Proposed interleaved DC-DC boost converter circuit

The interleaving technique is based on the paralleling technique whereby two or more converters are connected in parallel, thus dividing the input current among the inductors. The I^2R losses and the current stress are minimized with reduced output current and voltage ripples [13]–[15]. The design calculations for various parameters of the IBC are given next [12], [13].
- Duty cycle: the PV array voltage V_{PV} is $561\ V$ and the DC link inverter voltage V_{DC}, is taken to be $695\ V$ and hence the duty cycle of the IBC is specified as (8):

$$D = \frac{V_{DC}-V_{PV}}{V_{DC}} = \frac{695-561}{695} = 0.1928 \qquad (8)$$

- Inductors L_1 and L_2: taking the IBC switching frequency as $20\ kHz$ to reduce the ripple current, the values of the two inductors L_1 and L_2 is obtained as in (9) and (10):

$$I_L = N_P \times I_m = 2 \times 8.29 = 16.58\ A \qquad (9)$$

where N_P, is the number of parallel-connected modules, I_m is the PV peak/maximum current.

$$L_1 = L_2 = \frac{V_{PV}D}{f\Delta i_L} = \frac{561\times0.1928}{(20\times10^3\times0.06\times16.58)} = 5.43\ mH \approx 6\ mH \qquad (10)$$

where Δi_L is the ripple current of value 6% of I_L.

- Capacito$r$ C of DC link: the DC link capacitor C value is computed as in (11), taking $\omega = 2\pi f = 2\pi \times 50 = 314.1592\ rad/sec$.

$$C = \frac{I_{DC}}{6\times\omega\times\Delta V_{DC}} = \frac{17}{6\times314.1592\times0.06\times695} = 216.3\mu F \approx 220\mu F \qquad (11)$$

The suggested IBC simulation diagram was built within MATLAB and Simulink environment with the ANFIS-PID MPPT algorithms for both solar PV and WECS within the microgrid. The input voltage is taken to be $V_{in}=561\ V$, the switching frequency is $20\ kHz$, the duty ratio is $D = 0.1928$ and a resistive load $R=36\ \Omega$.

2.5. Transfer function model of photovoltaic-wind hybrid microgrid

The microgrid TF model is developed to support the performance study of the proposed ANFIS-PID controller in regulating the microgrid's voltage within the context of transient response. The mathematical TF models for a PV plant, WT generator, and BESS have been treated as lagging systems of the first-order having gains $(K_{PV}, K_{WTG}, K_{BESS})$ and time constants $(T_{PV}, T_{WTG}, T_{BESS})$ [27]. The individual subsystem TFs and related parameters are presented in Table 1 [26], [28]. The microgrid's schematic diagram has been transformed into a controlled equivalent TF model viewed in a small-signal-based dual voltage-current (V/I) controller TF model, as shown in Figure 3 [28].

Table 1. The individual subsystem mathematical TF models and related parameters [26], [28]

| Subsystem	TF	Parameters
Solar PV plant/wind turbine generator (WTG)	$G_{PV} = \frac{K_{PV}}{sT_{PV}+1}, G_{WTG} = \frac{K_{WTG}}{sT_{WTG}+1}$	$K_{PV} = 1, T_{PV} = 0.03s, K_{WTG} = 1, T_{WTG} = 1.5s$
DC-DC boost converter (BC)/buck-boost converter (BBC)	$G_{BC1} = \frac{K_{BC1}}{sT_{BC1}+1}, G_{BBC} = \frac{K_{BBC}}{sT_{BBC}+1}$	$K_{BC1} = 2.5, T_{BC1} = 0.01s, K_{BBC} = 1.5, T_{BBC} = 0.1s$
BESS	$G_{BESS} = \frac{K_{BESS}}{sT_{BESS}+1}$	$K_{BESS} = 1.8, T_{BESS} = 0.001s$
Inverter/microgrid system	$G_M = \frac{K_M}{2sH + D}$	$K_M = 1.8, H = 2, D = 0.015\ pu/Hz, = 0.085\ pu.s$
Load	$G_L = \frac{K_L}{sT_L+1}$	$K_L = 2, T_L = 0.04s$
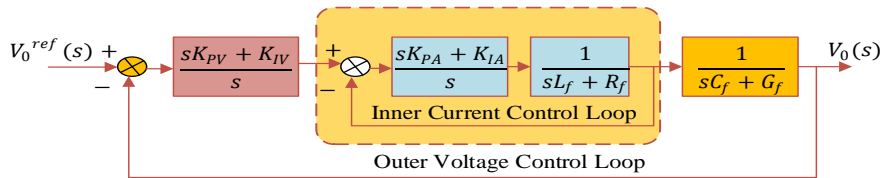
Figure 3. Nested voltage-current (V/I) controlled microgrid [28]

The overall TF from the input to the output was obtained using the block diagram reduction procedure and model-based pole-zero cancellation (MPZC) under small-signal as indicated by (12) [28]:

$$\left\{ \frac{V_0(s)}{V_0{}^{ref}(s)} = \frac{(K_{PA}K_{PV})s^2+(K_{IV}K_{PA}+K_{PV}K_{IA})s+K_{IA}K_{IV}}{\left(\begin{array}{c}(L_fC_f)s^4+(R_fC_f+G_fL_f+K_{PA}C_f)s^3+(G_fR_f+K_{PA}G_f+K_{PA}K_{PV}+C_fK_{IA})s^2) \\ (K_{IA}K_{PA}+G_fK_{IA}+K_{IV}K_{PA})s+K_{IA}K_{IV}\end{array}\right)} \right. \tag{12}$$

Applying MPZC by setting conductance used for filter design, $G_f = 0$, the voltage controller Integral gain, $K_{IV} = 0$, and the filter parameter (C_f) and the resultant computed values in Table 2, the ultimate is given in (13) for MPZC [28]:

$$\left\{ \frac{V_0(s)}{V_0{}^{ref}(s)} \right|^{MPZC} = \frac{s+56.08}{0.001s^3+0.163s^2+5.97s+56.08} \tag{13}$$

Table 2. Parameters used for the V/I controller equivalent TF [28]

Parameter	Description	Specification
C_f	Filter capacitance	$50\ \mu F$
L_f	Filter inductance	$1.35\ mH$
R_f	Filter resistance	$0.1\ \Omega$
K_{PA}	Current controller proportional gain	0.12
K_{IA}	Current controller integral gain	6.7
K_{PV}	Voltage controller proportional gain	$5.65e^{-4}$

2.6. Proportional integral/proportional-integral-derivative controller

The PI/PID controller optimum gains were obtained using the Ziegler-Nichols method and the MATLAB PID auto-tuning tool as $K_p = 1.77, K_I = 31.74, K_D = 0.016$ and filter coefficient, $N = 2558.64$. The contribution of the derivative term of the PID controller was minimal; hence, the controller action was very close to PI having $K_p = 1.61, K_I = 29.79$.

2.7. Adaptive neuro-fuzzy inference system controller

The ANFIS control structure utilizes the Sugeno-type fuzzy systems [22]. The structure consists of a collection of units organized into five interconnected layers [23], [24] that are tuned automatically by the hybrid learning algorithm. The significance of each layer and detailed operation of the 2-input-1-output ANFIS structure is presented in [22]. The flowchart of Figure 4 shows the ANFIS-PID algorithm.
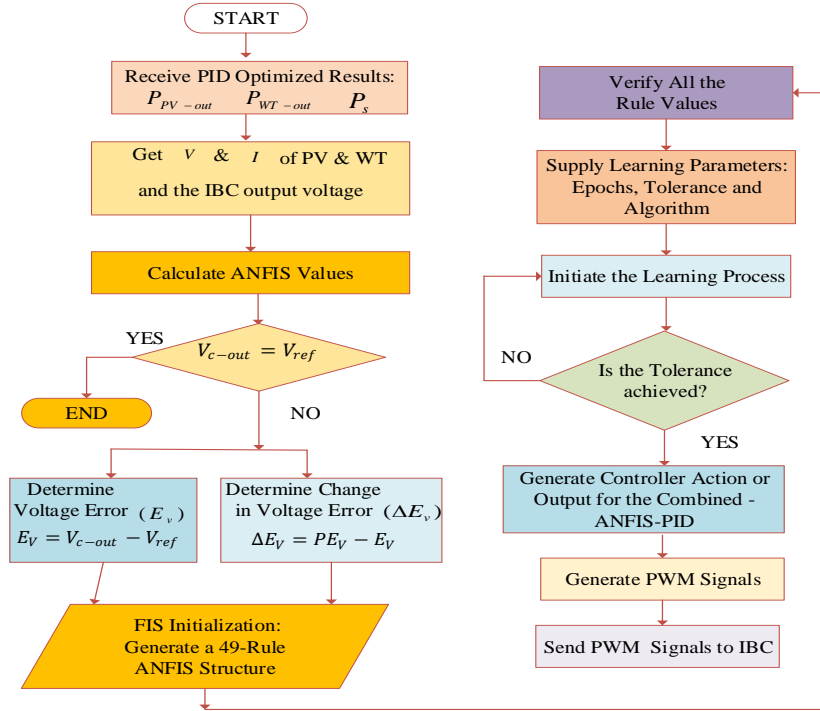

Figure 4. Flowchart of ANFIS-PID controller design

The PID output and the voltage error signals are presented to the ANFIS alongside the measured values of V and I and the required output voltage of the DC-DC converter. The set reference voltage is then computed from preset conditions. A comparison is made between the output voltage of the DC-DC converter (V_{c-out}) and set microgrid DC voltage (V_{ref}), and no action is taken if equal. However, if the (V_{c-out}) and V_{ref}, are unequal, the voltage error (E_v) and voltage error change (ΔE_v) are obtained from the previous voltage error (PE_v). The ANFIS-PID controller outputs a control signal if the tolerance/criteria are met, which is fed to the pulse width modulated (PWM) module. The PWM module produces PWM signals to regulate and stabilize the DC-DC converter output voltage. Supervised learning was used in the ANFIS design because labeled training data was available. The data was obtained from the designed model run with the PID controller and a MATLAB code, according to the generation data available at the national renewable energy laboratory (NREL) site [20]. The parameters of the designed integrated ANFIS-PID controller are shown in Table 3.

Table 3. ANFIS-PID system parameters

PI parameters	
$K_p = 1.61, K_I = 29.79$	
PID parameters	
$K_p = 1.77, K_I = 31.74, K_D = 0.016$ and filter coefficient $N = 2558.64$	
ANFIS parameters	
Number of nodes/linear parameters/nonlinear parameters	115/147/224
Total number of parameters	371 (premise=28, consequent=349)
Number of training/checking/testing data pairs	54 (57.4%)/20 (21.3%)/20 (21.3%)
Number of fuzzy rules	49
Training method	Hybrid learning algorithm
Designated epoch number/ANFIS training error tolerance	50/0.001

2.8. Combined Simulink model with case study

Figure 5 shows the TF-based Simulink diagram of the PV-wind hybrid microgrid with IBC. The consolidated 10 kW microgrid case study model of Figure 6 was obtained by integrating the individual models for the 10 kW solar PV system, the 10 kW wind energy system, the designed IBCs, and the BESS.
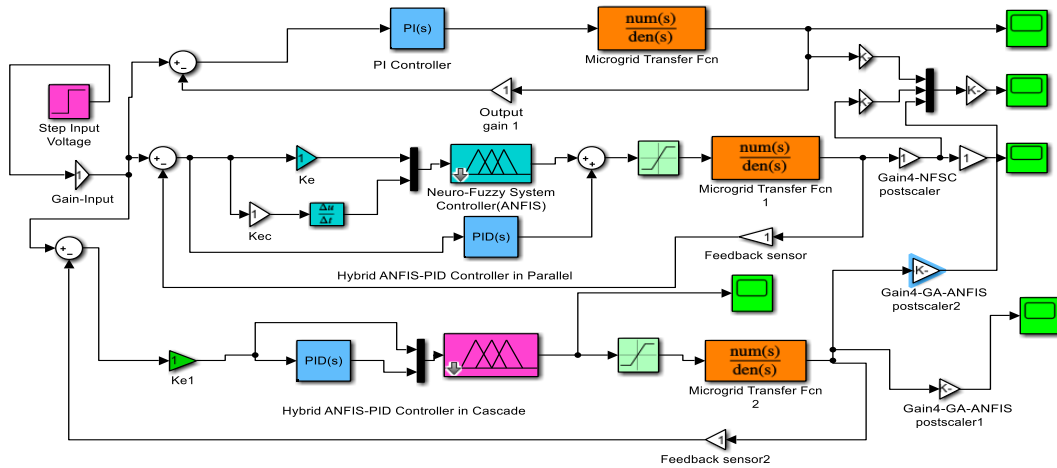

Figure 5. TF-based Simulink diagram of the PV-wind hybrid microgrid with IBC
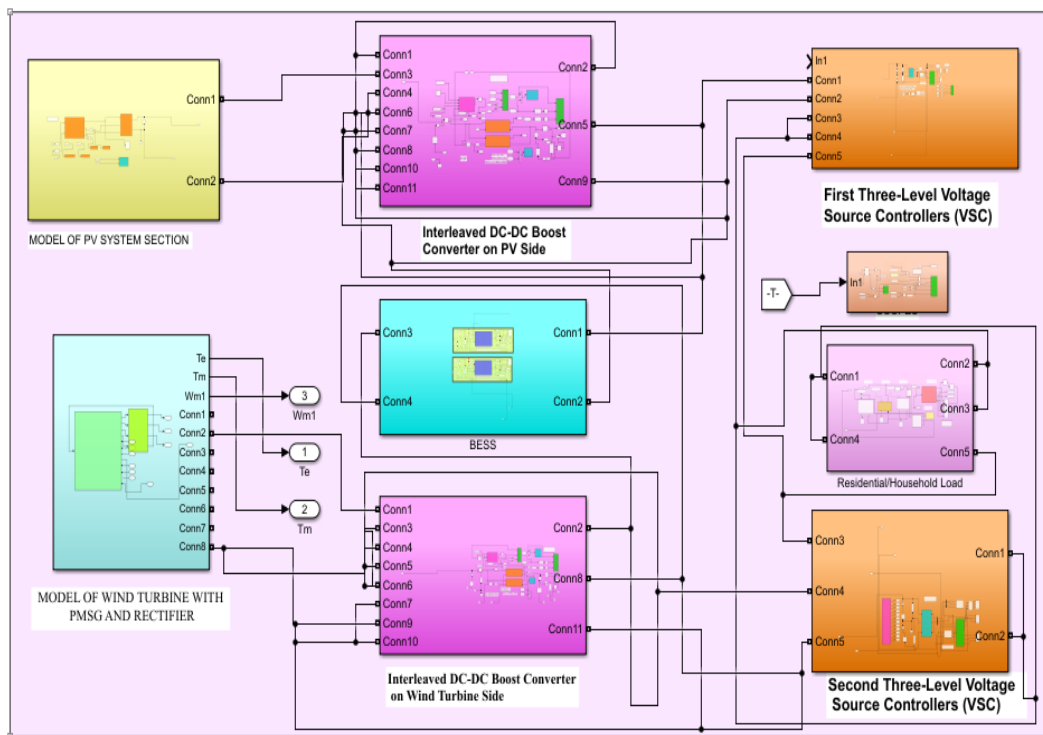

Figure 6. Simulink model of the microgrid case study with IBC

3. RESULTS AND DISCUSSION

3.1. Results from the interleaved boost converter-based microgrid transfer function model

Figure 7 depicts the response of various controllers to step change for the microgrid TF model. From the results in Figure 7, ANFIS-PID (parallel) controller recorded the best performance. The performance of PI, ANFIS-PID (cascade), and ANFIS-PID (parallel) controllers were tested with other voltage changes, and the voltage regulation capabilities obtained were summarized in Table 4.
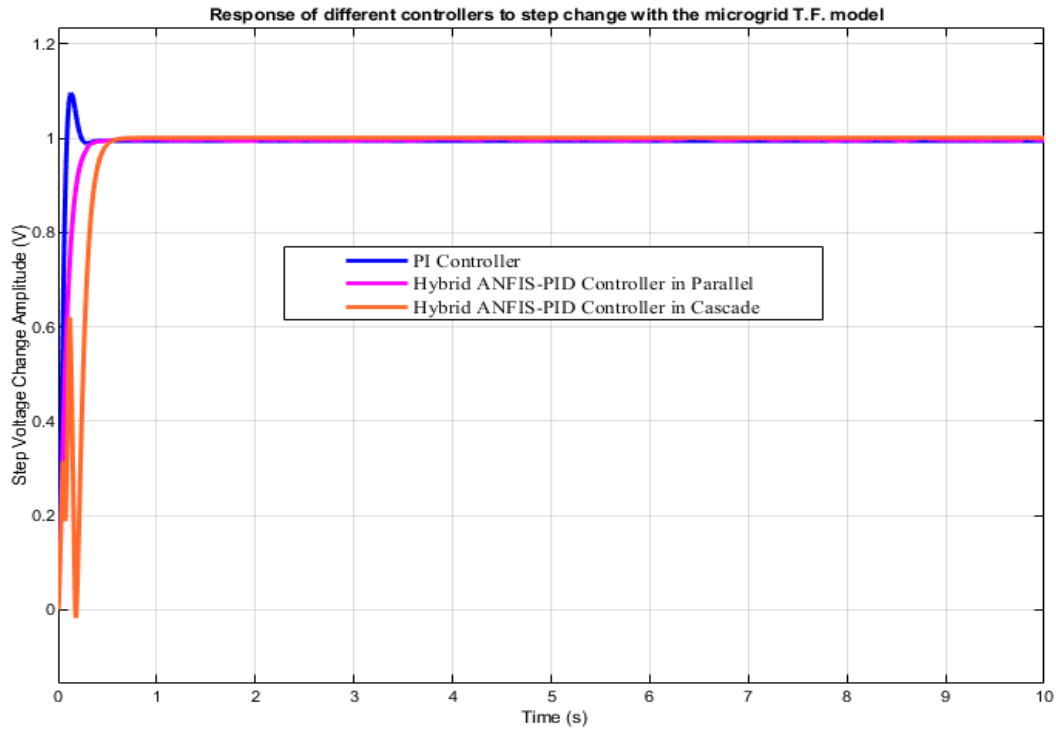
Figure 7. Response of different controllers to step change with the microgrid TF model

Table 4. PI, ANFIS-PID (cascade), and ANFIS-PID (parallel) controllers with various voltage changes

Step input	PI			ANFIS-PID (Cascade)			ANFIS-PID (Parallel)		
(V)	$t_r (s)$	$t_s (s)$	$M_p (\%)$	$t_r (s)$	$t_s (s)$	$M_p (\%)$	$t_r (s)$	$t_s (s)$	$M_p (\%)$
1	0.1	0.3	10.0	0.3	0.5	0.0	0.1	0.2	0.0
5	0.1	0.3	10.0	0.3	0.5	0.0	0.1	0.2	0.0
10	0.1	0.4	11.0	0.2	0.6	0.0	0.1	0.1	0.0
Avg.	0.10	0.33	10.33	0.27	0.56	0.00	0.10	0.17	0.00

The results obtained with various voltage step inputs indicated that the hybrid ANFIS-PID responds with the fastest settling time (t_s), shortest rise time (t_r) and smallest maximum overshoot (M_p). The ANFIS-PID (cascade) has t_r of 0.27 s, t_s of $0.56\ s$ and M_p of 0%; the ANFIS-PID (parallel) has t_r of 0.10 s, t_s of $0.17\ s$ and M_p of 0%, while the PI control has t_r of 0.10 s, t_s of $0.33\ s$ and M_p of 10.33%. The value of M_p for either topology of ANFIS-PID is zero, but for the PI controller, it is 10.33%, which is above the voltage limits of $\pm 5\%$ specified by the IEEE-1547 and IEEE-519 standards. The system tends to best track the new set voltage points with the parallel form of the ANFIS-PID having smaller t_r and t_s than for ANFIS-PID (cascade). The ANFIS-PID controller also has the best prediction, learning capability, and ability to cope with nonlinearities associated with the microgrid. However, the PI controller does not have the learning and prediction capability of the ANFIS-PID and struggles with nonlinearities in the microgrid.

3.2. Results from the interleaved boost converter-based microgrid Simulink case study model

The proposed IBC inputs in the case study model are voltage $V_{in} = 561\ V$ and current, $I_{in} = 26\ A$ at a switching frequency of $20\ kHz$ and the duty ratio $D = 0.1928$. The IBC output voltage of $678 \pm 20\ V$ ($\pm 3.0\%$) and current obtained with PI-controller is shown in Figure 8, and with ANFIS-PID (parallel) controller in Figure 9 that displays a voltage output of $675 \pm 15\ V$ ($\pm 2.2\%$). The ANFIS-PID regulated the IBC output voltage to within $\pm 2.22\%$ of the nominal $675\ V$, which is well within the required $\pm 5\%$, giving a better voltage profile than PI, whose overshoot is 3.0%. Figures 10 and 11 show the BESS output voltage, SoC, and current with the conventional PI and ANFIS-PID controllers in the proposed IBC-based case study microgrid model. Although some ripples or overshoot of 2.2% were noted with the ANFIS-PID, it was still lower than the 3.0% recorded with the PI.
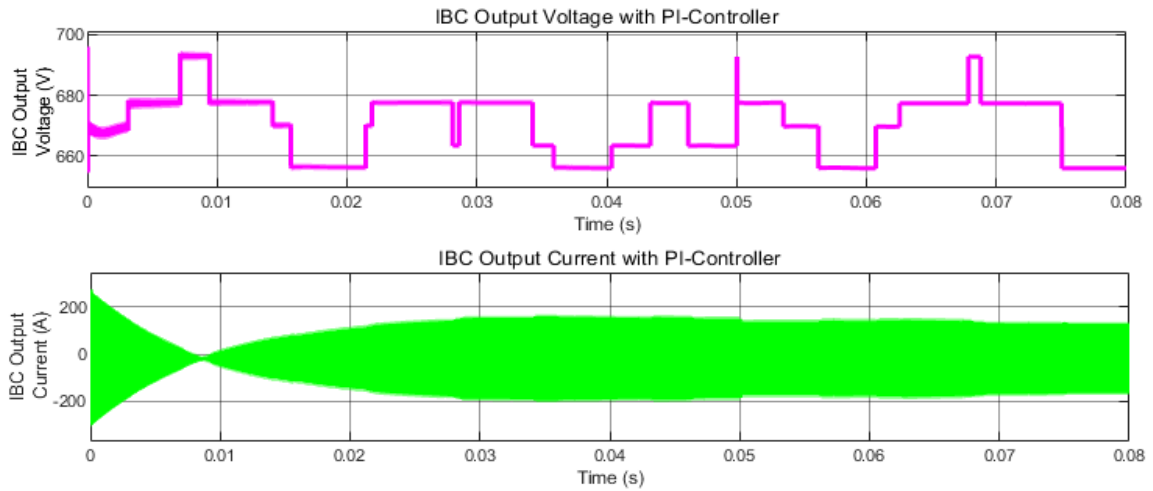
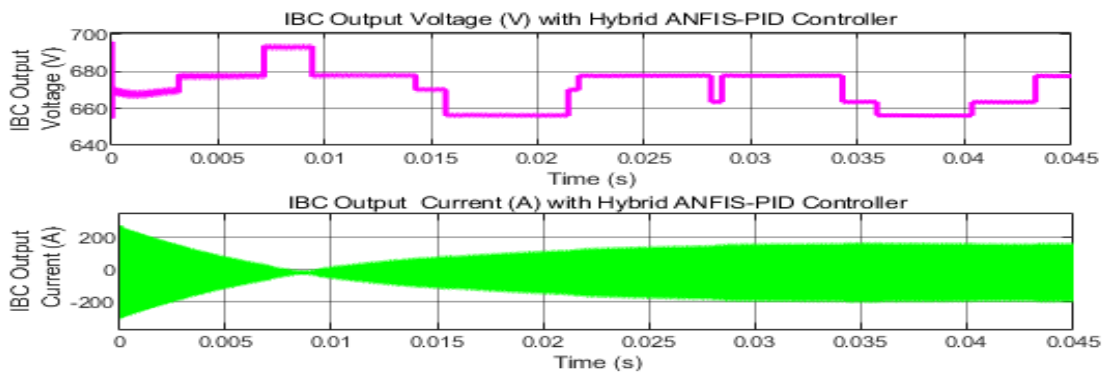Figure 8. IBC output voltage and output current with PI controller

Figure 9. IBC output voltage and output current with hybrid ANFIS-PID controller
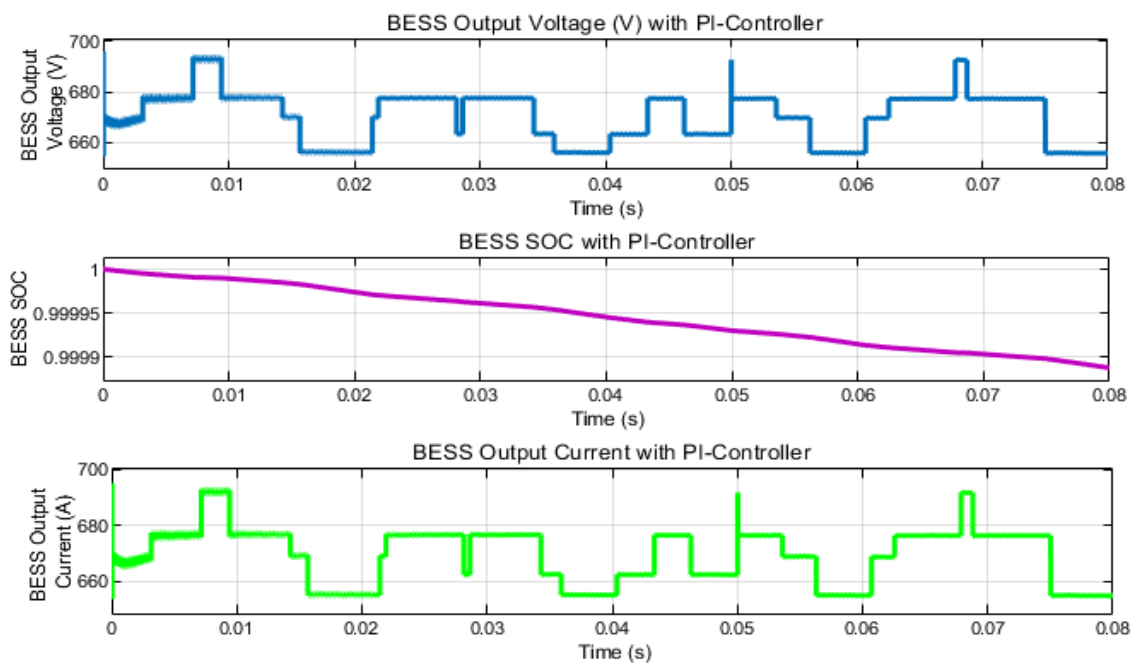

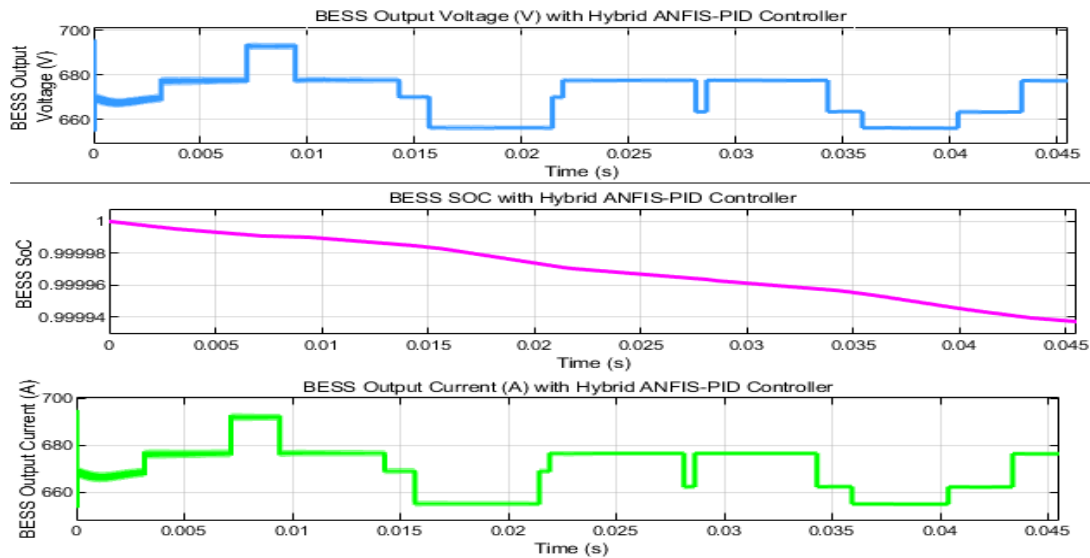Figure 10. BESS output voltage, SoC, and current with PI controller

Figure 11. BESS output voltage, SoC, and current with ANFIS-PID controller

4. CONCLUSION

This paper has developed a unique model of IBC for an off-grid hybrid 10 kW PV-wind microgrid using an interleaving technique in MATLAB/Simulink and designed an ANFIS-PID controller for voltage regulation. The study's main contributions include the developed IBC model and the ANFIS-PID controller used to optimize the IBC outputs in the microgrid. Further, a PI controller was used to validate the performance of the ANFIS-PID controller both on a TF microgrid model and on the Simulink case study model by tracking the desired voltage outputs. This research has found that the ANFIS-PID approach provided the best performance compared to the conventional PI controller. The ANFIS-PID (parallel) controller registered a rise time of $0.10\ s$, settling time of $0.17\ s$, and zero overshoot compared to the $0.10\ s$, $0.33\ s$, and 10.33% for the PI controller, respectively. The ANFIS-PID controller also significantly reduced the distortions in the microgrid's voltage and current plots of the IBC. Future work can investigate whether the designed ANFIS-PID controller's performance can be improved by hybridizing it further using the third algorithm.

REFERENCES

[1] L. A. Aloo, P. K. Kihato, S. I. Kamau, and R. S. Orenge, "Model predictive control-adaptive neuro-fuzzy inference system control strategies for photovoltaic-wind microgrid: feasibility review," in *2020 IEEE PES/IAS PowerAfrica*, Aug. 2020, pp. 1–5, doi: 10.1109/PowerAfrica49420.2020.9219853.

[2] S. Sumathi, L. A. Kumar, and P. Surekha, *Solar PV and wind energy conversion systems*, 1st ed. Cham: Springer International Publishing, 2015, doi: 10.1007/978-3-319-14941-7.

[3] M. Jayachandran and G. Ravi, "Design and optimization of hybrid micro-grid system," *Energy Procedia*, vol. 117, pp. 95–103, Jun. 2017, doi: 10.1016/j.egypro.2017.05.111.

[4] I. Yahyaoui, *Advances in renewable energies and power technologies: volume 1: solar and wind energies*. Amsterdam: Elsevier, 2018, doi: 10.1016/C2016-0-04919-7.

[5] A. Khalil, K. A. Alfaitori, and A. Asheibi, "Modeling and control of PV/wind microgrid," in *2016 7th International Renewable Energy Congress (IREC)*, Mar. 2016, pp. 1–6, doi: 10.1109/IREC.2016.7478916.

[6] G. Maślak and P. Orłowski, "Microgrid operation optimization using hybrid system modeling and switched model predictive control," *Energies*, vol. 15, no. 3, pp. 1–21, Jan. 2022, doi: 10.3390/en15030833.

[7] M. M. Jouzdani, M. Shaneh, and T. Nouri, "Design of an interleaved high step-up DC-DC converter with multiple magnetic devices for renewable energy systems applications," *International Transactions on Electrical Energy Systems*, pp. 1–14, Jun. 2022, doi: 10.1155/2022/2645938.

[8] A. Kokate, H. Khandagale, J. George, A. Koli, and S. Nair, "Modeling and simulation of standalone wind energy conversion system," in *2019 3rd International Conference on Trends in Electronics and Informatics (ICOEI)*, Apr. 2019, pp. 1295–1297, doi: 10.1109/ICOEI.2019.8862682.

[9] S. Amara, S. Toumi, and C. ben Salah, "Modeling and simulation of hybrid renewable microgrid system," in *2020 17th International Multi-Conference on Systems, Signals & Devices (SSD)*, Jul. 2020, pp. 1074–1079, doi: 10.1109/SSD49366.2020.9364193.

[10] J. Meng, G. Luo, M. Ricco, M. Swierczynski, D.-I. Stroe, and R. Teodorescu, "Overview of lithium-ion battery modeling methods for state-of-charge estimation in electrical vehicles," *Applied Sciences*, vol. 8, no. 5, pp. 1–17, Apr. 2018, doi: 10.3390/app8050659.

[11] O. Abdel-Rahim and H. Wang, "A new high gain DC-DC converter with model-predictive-control based MPPT technique for photovoltaic systems," *CPSS Transactions on Power Electronics and Applications*, vol. 5, no. 2, pp. 191–200, Jun. 2020, doi: 10.24295/CPSSTPEA.2020.00016.

[12] K. Faraj and J. Hussain, "Analysis and comparison of DC-DC boost converter and interleaved DC-DC boost converter," *Engineering and Technology Journal*, vol. 38, no. 5, pp. 622–635, May 2020, doi: 10.30684/etj.v38i5A.291.

[13] R. D. Tayade and S. S. Mopari, "Comparative analysis of interleaved boost converter and CUK converter for solar powered BLDC motor," *International Journal of Electrical and Electronics Engineering (IJEEE)*, vol. 6, no. 4, pp. 1–12, 2017, [Online]. Available: http://www.iaset.us/view_archives.php?year=2017&jtype=2&id=15&details=archives

[14] P. Prabhakaran and V. Agarwal, "Novel boost-SEPIC type interleaved DC–DC converter for mitigation of voltage imbalance in a low-voltage bipolar DC microgrid," *IEEE Transactions on Industrial Electronics*, vol. 67, no. 8, pp. 6494–6504, Aug. 2020, doi: 10.1109/TIE.2019.2939991.

[15] C. Hisar, "Three-phase parallel interleaved boost converters," *MathWorks*, 2019. https://www.mathworks.com/matlabcentral/fileexchange/72749-three-phase-parallel-interleaved-boost-converters (accessed Aug. 16, 2022).

[16] K. Özel and A. Karaaslan, "The design of standalone PV system using P&O algorithm for maximum power point tracking," *Communications Faculty of Sciences University of Ankara Series A2-A3 Physical Sciences and Engineering*, vol. 62, no. 1, pp. 14–25, 2020, doi: 10.33769/aupse.559971.

[17] A. A. AlZubaidi, L. A. Khaliq, H. S. Hamad, W. K. Al-Azzawi, M. S. Jabbar, and T. A. Shihab, "MPPT implementation and simulation using developed P&O algorithm for photovoltaic system concerning efficiency," *Bulletin of Electrical Engineering and Informatics*, vol. 11, no. 5, pp. 2460–2470, Oct. 2022, doi: 10.11591/eei.v11i5.3949.

[18] A. Tounsi, H. Abid, M. Kharrat, and K. Elleuch, "MPPT algorithm for wind energy conversion system based on PMSG," in *2017 18th International Conference on Sciences and Techniques of Automatic Control and Computer Engineering (STA)*, Dec. 2017, pp. 533–538, doi: 10.1109/STA.2017.8314957.

[19] M. A. Fouad, M. A. Badr, and M. M. Ibrahim, "Modeling of micro-grid system components using MATLAB/SIMULINK," *International Journal of Signal System Control and Engineering Application*, vol. 12, no. 4, pp. 93–104, 2017, doi: 10.36478/ijssceapp.2019.93.104.

[20] National Renewable Energy Laboratory (NREL), "System advisor model version 2017.9.5 (SAM 2017.9.5)," *National Renewable Energy Laboratory (NREL)*. https://sam.nrel.gov/download/version-2017-9-5.html (accessed Jul. 29, 2022).

[21] S. Kumar, "Battery charging and discharging model," *MathWorks*, 2012. https://www.mathworks.com/matlabcentral/fileexchange/38304-battery-charging-and-discharging-model. (accessed Jun. 09, 2022).

[22] K. A. A. Sumarmad, N. Sulaiman, N. I. A. Wahab, and H. Hizam, "Energy management and voltage control in microgrids using artificial neural networks, PID, and fuzzy logic controllers," *Energies*, vol. 15, no. 1, pp. 1–22, Jan. 2022, doi: 10.3390/en15010303.

[23] D. Gamage, X. Zhang, A. Ukil, C. Wanigasekara, and A. Swain, "Design of ANFIS controller for a DC microgrid," in *2020 3rd International Conference on Energy, Power and Environment: Towards Clean Energy Technologies*, Mar. 2021, pp. 1–6, doi: 10.1109/ICEPE50861.2021.9404439.

[24] D. N. Truong, V. T. Ngo, M. S. N. Thi, and A. Q. Hoang, "Application of an adaptive network-based fuzzy inference system to control a hybrid solar and wind grid-tie inverter," *Engineering, Technology & Applied Science Research*, vol. 11, no. 5, pp. 7673–7677, Oct. 2021, doi: 10.48084/etasr.4413.

[25] N. Pawar and P. Nema, "Anfis based forecast model for predicting PV energy generation system," *International Journal of Scientific and Technology Research*, vol. 9, no. 3, pp. 6517–6523, 2020.

[26] M. Ali, H. Kotb, K. M. Aboras, and N. H. Abbasy, "Design of cascaded PI-fractional order PID controller for improving the frequency response of hybrid microgrid system using gorilla troops optimizer," *IEEE Access*, vol. 9, pp. 150715–150732, 2021, doi: 10.1109/ACCESS.2021.3125317.

[27] D. Kumar, H. D. Mathur, S. Bhanot, and R. C. Bansal, "Modeling and frequency control of community micro-grids under stochastic solar and wind sources," *Engineering Science and Technology, an International Journal*, vol. 23, no. 5, pp. 1084–1099, Oct. 2020, doi: 10.1016/j.jestch.2020.02.005.

[28] Y. V. P. Kumar and R. Bhimasingu, "Design of voltage and current controller parameters using small signal model-based pole-zero cancellation method for improved transient response in microgrids," *SN Applied Sciences*, vol. 3, no. 11, pp. 1–17, Nov. 2021, doi: 10.1007/s42452-021-04815-x.

BIOGRAPHIES OF AUTHORS

Linus Alwal Aloo holds a B.Sc. Degree in Electrical and Electronic Engineering (2013), and a Master's Degree in Electrical Engineering (2018), both from Jomo Kenyatta University of Agriculture and Technology, JKUAT (Kenya), and is currently pursuing a Ph.D. in Electrical Engineering at JKUAT. His research interests are microgrid control, artificial intelligence techniques, control systems design, iot-based smart systems, and renewable energy. He can be contacted at email: laloo@jkuat.ac.ke.

Peter Kamita Kihato holds M.Sc. Degree in Electrical Engineering (Tottori University, Japan) and a Ph.D. Degree (2010) in Electrical Engineering from JKUAT (Kenya) and Tottori under a split program. He is currently a Senior Lecturer with the Department of Electrical and Electronic Engineering, JKUAT. His research interests include artificial intelligence techniques, microcontroller applications, embedded systems, power system automation, and renewable energy. He can be contacted at email: pkihato@jkuat.ac.ke.

Stanley Irungu Kamau received the B.Sc. Degree in Electrical Engineering from Moi University, Kenya, in 1990, the M.Eng.Sc. Degree in Electrical Engineering from the University of New South Wales, Australia, in 1993, and the Dr. Ing. Degree in Electrical Engineering from Ruhr-Universität Bochum, Germany, in 2004. He is currently a Professor with the Department of Electrical and Electronic Engineering, JKUAT. His research interests include hybrid control systems, real-time control, microgrid control, and renewable energy development. He can be contacted at email: skamau@eng.jkuat.ac.ke.

Roy Sam Orenge received his B.Sc. Degree in Electrical and Electronic Engineering (2011) from JKUAT (Kenya), a Master's Degree (2014), and Ph.D. Degree (2019) in Electrical Engineering from Pan African University Institute for Basic Sciences, Technology, and Innovation (PAUSTI). He is a registered Professional Engineer with the Engineers' Board of Kenya (EBK). His research areas are electrical power system modeling and design, renewable energy systems and grid integration, rural electrification and off-grid systems, and electrical machines. He can be contacted at email: roy.orenge@jkuat.ac.ke.